MAGNETICALLY CONTROLLED STRUCTURES

IN THE IONOSPHERE OF MARS

by

Firdevs Duru

A thesis submitted in partial fulfillment
of the requirements for the Master of
Science degree in Physics
in the Graduate College of
The University of Iowa

July 2006

Thesis Supervisor: Professor Donald A. Gurnett

To my mom Zuhal Duru, to my dad Ismail Hakki Duru and to my sister Nadire Duru

ACKNOWLEDGMENTS

ABSTRACT

The ionospheric sounding data obtained by the MARSIS (Mars Advanced Radar for Subsurface and Ionospheric Sounding) instrument on the Mars Express spacecraft shows that the dayside ionosphere has considerable structure over regions of strong crustal magnetic fields. This structure is typically seen as hyperbola-shaped echoes in a display of echo intensity versus apparent altitude and time. The hyperbola shapes of the echoes are consistent with oblique reflections from regions of enhanced electron density fixed with respect to Mars. Comparisons with the Cain et al. [2003] model for the crustal magnetic field of Mars show that the apexes of the hyperbolas, which identify the approximate center of the regions of enhanced electron density, usually coincide with regions where the crustal magnetic field is nearly vertical. The electron densities enhancements, which extend as much as 50 km above the surrounding ionosphere, are believed to arise from increases in the scale height of the ionosphere, possibly due to heating of the ionosphere by solar wind electrons that reach the base of the ionosphere along nearly vertical (open) magnetic field lines. Statistical analyses of the apparent altitudes of the apexes of the hyperbolas, as well as analyses of repeated passes over the same region, indicate that the electron density enhancements consist of horizontal linear structures rather than isolated point-like structures. In some cases the axes of the linear density structures are found to be aligned along the axes of cylindrical magnetic field structures in the crustal magnetic field of Mars.

TABLE OF CONTENTS

LIST OF FIGURES

Figure

CHAPTER I
INTRODUCTION

The Mars Express spacecraft was launched in June 2, 2003 from Baikonur, Kazakhstan and entered an elliptical orbit around Mars on December 25, 2003 [Chicarro et al., 2004]. Mars Express carries a low-frequency radar called MARSIS (Mars Advanced Radar for Subsurface and Ionospheric Sounder) that is designed to provide subsurface radar soundings and to study the ionosphere of Mars [Picardi et al., 2004]. The data collected by MARSIS provide the first radar soundings of Mars. Initial reports on the subsurface and ionospheric soundings results from MARSIS were published by Picardi et al. [2005] and Gurnett et al. [2005]. One of the unanticipated results from the ionospheric sounding was the discovery of oblique echoes from electron density structures that are associated with the crustal magnetic fields discovered by the Mars Global Surveyor spacecraft [Acuna et al., 1998, 1999; Connerney et al., 2001]. The purpose of this thesis is to expand on these early results by studying the location and geometry of the electron density structures responsible for the oblique echoes and to study their relationship to the crustal magnetic fields of Mars.

The first in-situ investigations of the ionosphere of Mars were obtained by the Viking 1 and 2 landers. The first lander reached the surface of Mars on July 20, 1976 and the second one touched down on September 3, 1976. The electron density and temperature profiles were obtained from retarding potential analyzers (RPAs) which were mounted on the aeroshell of the landers [Hanson et al., 1977; Hanson and Mantas, 1988]. The two plots in Figure 1 from Hanson et al., [1977] show the observed ion concentration profiles from Viking 1 and 2 landers. On Viking 2 it was possible to observe more structure in the height profiles of ionospheric quantities, but the results were similar to

the Viking 1 profiles. In both cases, it was possible to determine the total ion concentration and it was observed that O^{2+} is the most abundant ion on the ionosphere of Mars along with significant quantities of CO^{2+} and O^+ [Hanson et al., 1977]. The thermal electron temperature (T_e) in the upper Martian ionosphere was found to be several thousand degrees Kelvin and it was concluded that solar wind is an important energy and suprathermal electron source to the topside of the ionosphere [Hanson and Mantas, 1988]. Since the Viking landers did not carry instruments for measuring magnetic fields, they could not provide data on the magnetic field structure of Mars [Luhmann and Brace, 1991]. However, according to the Viking data, the ionospheric plasma pressure – including the ions and suprathermal electrons- is much smaller than the average solar wind dynamic pressure, indicating that a magnetic field of at least $30 - 40$ nT is required to compensate for the missing pressure [Hanson and Mantas, 1988; Shinagawa and Bougher, 1999].

More recently, radio occultation measurements using several US and Russian satellites (such as Mariner) supplemented our knowledge about the ionosphere of Mars by providing electron density profiles of the Mars ionosphere at the altitudes between 120-300 km [Zhang et al., 1990a, 1990b]. According to the radio occultation data, the dayside peak electron densities of Mars exhibit ideal Chapman layer-like behavior. The altitude of the ionospheric peak increases while the density decreases with the solar zenith angle (SZA), which is defined as the angle between the local zenith of the satellite and the line of sight to the sun [Zhang et al., 1990a, 1990b; Luhmann and Brace, 1991]. It was also found that most of the time the nightside electron density of the ionosphere of Mars is too weak to be detected by the radio occultation methods [Zhang et al., 1990b]. It

should be remembered that due to the respective positions of Mars and Earth, radio occultation measurements deep in the nightside of Mars are geometrically impossible.

Finally, the Mars Global Surveyor (MGS) experiment was the first spacecraft to obtain magnetic field observations close to Mars at altitudes around 170-200 km. One of the goals of this spacecraft was to detect and characterize the magnetic field of the planet and study the interaction of the atmosphere with the solar wind. The MGS carried a magnetometer and electron reflectometer (MAG/ER) package, and it could perform many low altitude measurements. The magnetometer provided in-situ sensing of the local magnetic field and an electron reflectometer was used to remotely measure the magnetic fields of planetary origin. The data obtained by MGS confirmed that Mars lacks an appreciable magnetic field of internal origin, as was proven by earlier studies. The fact that Mars does not have a core magnetic field was first shown by the results obtained by Mariner 4. During the encounter between Mars and Mariner 4 no magnetic effect that could be definitely associated with the planet was found in the magnetometer data. It was deduced that the Martian magnetic dipole moment is at most $3x\ 10^{-4}$ times that of the Earth [Smith et al., 1965; Van Allen et al., 1965]. MGS showed that Mars has strong, small scale, remnant crustal magnetic fields. The magnetic fields are highly localized and their magnitude reaches 400 nT in some areas. It is inferred that Mars once had an internal active dynamo that does not exist at the present time [Acuna et al., 1998, 1999].

The Cain et al. model [Cain et al., 2003] of the magnetic structure of Mars was created based on the information obtained by MGS. The data are modeled using algorithms originally developed for terrestrial data. This is done by deriving a potential function using spherical harmonics expansions to about a degree of n = 90 from a

selection of MGS data [Cain et al., 2003]. It also showed the presence of an ionopause and provided information on the electron spectrum.

CHAPTER II
INSTRUMENTATION

2.1 The Mars Express Spacecraft

Mars Express is the first European Space Agency (ESA) mission to fly to Mars. In addition to ESA member states other countries like the USA, Russia, Poland, Japan and China participated in the mission and provided the scientific payload. Figure 2 shows an artistic sketch of the Mars Express spacecraft which was launched from Baikonur on 2 June 2003 and entered an orbit around Mars on 25 December 2003 [Chicarro et al., 2004]. Although the orbit parameters have changed somewhat during the course of the mission, for the time period analyzed in this study, from July 11, 2005 to January 27, 2006, the periapsis altitude was about 275 km, the apoapsis altitude was about 10,100 km, the inclination was 86.35 degrees and the period was about 6.75 h. Figure 3 shows the orbit of the Mars Express Spacecraft.

The measurements which are being performed by Mars Express can be summarized as global color and stereo high-resolution imaging; global IR mineralogical mapping of the surface; radar sounding of the subsurface structure down to the permafrost, global atmospheric circulation and mapping of the atmospheric composition; interaction of the atmosphere with the surface and the interplanetary medium; and radio science. These measurements are designed to infer critical information on the atmosphere, ionosphere, surface and interior; organic and inorganic chemical analysis.

The Mars Express spacecraft carries six instruments: the PFS planetary fourier spectrometer, the SPICAM UV IR atmospheric spectrometer, the ASPERA energetic neutral atoms analyzer, the HRSC super/high resolution stereo colour imager, the OMEGA IR mineralogical mapping spectrometer and the MARSIS subsurface sounding

radar altimeter. The first three investigate the atmosphere and environment of the planet. The others study the planet by observing the surface and subsurface [A. Chicarro et al., 2004].

2.2 The Mars Advanced Radar for Subsurface and
Ionospheric Sounding (MARSIS)

MARSIS (Mars Advanced Radar for Subsurface and Ionospheric Sounding) is a low frequency radar sounder which transmits pulses and receives the corresponding echoes. MARSIS is used for radar sounding of the ionosphere as well as subsurface sounding. Its main objective is to map the distribution of water in the upper parts of the crust down to depths of 3-5 km. Other goals include subsurface geological probing, surface roughness and topography characterizations, and ionospheric sounding. The ionospheric sounding is used to understand the characteristics of the ionosphere and its interactions with the solar wind [A. Chicarro et al., 2004].

MARSIS consists of an antenna subsystem which has a 40 m tip-to-tip primary dipole antenna for transmission and reception of the sounder pulses and a 7 m secondary monopole antenna for surface-clutter echo rejection; a radio frequency subsystem containing both the transmitter and two digital receivers, one for the dipole antenna and one for the monopole antenna; a digital electronics subsystem that includes a signal generator, a timing and control unit and a processing unit.

MARSIS performs both passive (receive only) and active soundings. The passive mode makes in-situ measurements of the electron density from thermal emissions at the electron plasma frequency. In the active mode, a pulse is transmitted from MARSIS at a

frequency f and the intensity of the reflected radar echo is measured as a function of the time delay.

The electronic block diagram of the radar is shown in Figure 4. The transmit/receive cycle is repeated at a fixed rate under control of the Pulse Repetition Frequency system. The radar transmits pulses and receives the corresponding echoes. Of the five receiver bands (Figure 5) the first band is only for ionospheric sounding, the other four are for both ionospheric and subsurface soundings. The active mode performs ionospheric soundings on certain passes when the orbiter is at an altitude below 1200 km, both during the day time and night time. Sinusoidal pulses having a nominal duration of 91.4 μs are sent at 160 frequencies that span a range from 100 kHz to 5.5 MHz in an ascending time order [Picardi et al., 2004]. The pulse is transmitted once every 7.85 ms via the dipole antenna and the intensity of any returning echo is detected in a digitally constructed 10.9 KHz frequency band centered on the frequency of the transmitted pulse. The basic frequency scan is shown in Figure 6. The time delay of the echo is determined by sampling the received signal intensities in 80 equally spaced time bins extending from 0 to 73.1 ms after the transmitted pulse. The total frequency interval, 5400 kHz, is divided into 495 small intervals of 10.9 kHz each. Among these 495 frequency values, 160 frequency values which have an equal fractional frequency difference between them on a quasi - logarithmic scale (given by $\Delta f/f \approx 2$ %) are chosen. Some of these 160 frequency values have been replaced by nearby frequency values due to a high interference level from the spacecraft electronics at certain frequencies. A complete scan through all 160 frequencies takes 1.257 s, and the basic sweep cycle is repeated once every 7.54 s.

It is important to investigate the ionosphere of Mars both because relatively little is known about it and it has a strong influence on the subsurface and surface soundings. The top panel in Figure 7 shows a typical vertical profile of the electron plasma frequency f_p in the Martian ionosphere as a function of the altitude z. The bottom panel displays the corresponding time delay versus frequency plot for a given vertical profile. The electron plasma frequency is given by $f_p = 8980\sqrt{n_e}$ where n_e is the electron number density in cm^{-3}. Sounding is possible because the radio waves are reflected by the ionosphere at $f=f_p$. Reflection occurs because the free space electromagnetic mode cannot propagate through an ionized gas at frequencies below the electron plasma frequency [Gurnett et al., 2005]. When the wave frequency is equal to the f_p, radio waves incident vertically on the horizontally stratified ionosphere are reflected back to the spacecraft. Transmission through the ionosphere is possible only at frequencies above the maximum electron plasma frequency in the ionosphere. Even at frequencies above f_P (max) the ionosphere still has an effect on the radar signal because the index of refraction deviates from the free space value of n=1 [Picardi et al., 2004, Gurnett and Bhattacharjee, 2005]. This effect is called dispersion.

CHAPTER III
OVERVIEW OF THE DATA

3.1 Data Flow

The ionospheric data collection is strongly controlled by the elliptical geometry of the Mars Express orbit. The data are normally collected duing periapsis passes and transmitted near apoapsis as shown in Figure 3 [Picardi et al., 2004]. A typical ionospheric sounding pass lasts about 36 minutes and provides about 285 frequency scans. Because of gravitational perturbations, the local time and latitude of periapsis evolves rather rapidly. Most of the data analyzed in this paper have been obtained from the dayside of Mars.

Signals transmitted via the spacecraft's high gain antenna are received by ESA's ground receiving antennas which are operated by the European Space Operation Center (ESOC) in Darmstadt Germany. While communicating with ESOC, the Mars Express is not able to collect data since the high gain transmitting antenna must be pointed at the Earth. The primary 35 m disk receiving antenna which is located at New Norcia, Australia was used for the first time for the Mars Express mission. So far, all the planned operations have been successfully executed. To increase the ability to receive data, a secondary 35 m dish antenna has been put into operation at Cerberos, near Madrid, Spain. The Cerberos antenna is currently providing backup support for Mars Express. The received data are processed into Level 1a science data packets (which are the cleaned, time-ordered, packet-formatted data that have been separated by instrument) and can be accessed via Mars Express Data Distribution System (DDS). The ASI (Agenzia Spaziale Italiana – Italian Space Agency) Science Data Center (ASDC) at Frascati, Italy, performs further processing.

The Level 1a instrumental data files and Level 1b ionospheric data files (which are the Level 1a data sorted by instrument data types and instrument modes in a scientifically useful form) along with any other appropriate ancillary data files are automatically transferred to the Iowa MARSIS processing facility on a regular basis via the data mirroring function. Then, standard (Level 2) ionospheric data products (calibrated electric fields values, displays used to analyze data) are generated. Finally, higher level ionospheric data products are created (such as f_p values) depending on the analyses.

3.2 MARSIS Data Displays

The data received from MARSIS are displayed in different forms of ionospheric data products which make the analysis easier. The types of data displays used in this study are as follows:

3.2.1 Ionograms

An ionogram is a color-coded display of the received echo strength versus frequency and time delay (Figure 8). Time delay is plotted on the vertical axis and is increasing downward. In Figure 8 a well-defined ionospheric echo can be seen ranging from about 0.5 to 1.7 MHz at a time delay around 4.25-5 ms. The echo ranging from about 1.7 to 5.5 MHz at around 5.5 ms is the ground reflection. The ionospheric echo and ground reflection usually form a cusp at the value of the maximum plasma frequency. This is because the group velocity, $v_g = c[1 - (f_p/f)^2]^{1/2}$, approaches zero over an increasingly long path length as the frequency approaches the maximum plasma

frequency. As a consequence, the time delay, which is given by $t = 2\int_0^h dz/v_g$, becomes

very large and results in a cusp on an ionogram.

The second ionospheric echo directly below the first ionospheric echo (at a time

delay around 6.5 ms) is a new unexpected echo and is believed to be caused by an

oblique reflection. As we will show, the positions of the oblique echoes correspond to

enhanced electron density regions that are fixed with respect to Mars. The vertical lines at

the top of the ionogram are electron plasma oscillation harmonics. Sometimes it is

possible to see periodic horizontal lines along the left side of the ionograms. Those are

electron cyclotron echoes which are believed to be caused by the electrons accelerated by

the strong electric field near the antenna. [Gurnett et al., 2005].

3.2.2 Spectrograms

Among several types of plots used for analyzing the ionospheric sounding data, a

color-coded spectrogram that gives echo strength at a fixed frequency as a function of

apparent altitude, h, and Universal Time (UT) is particularly useful. Apparent altitude is

the altitude at which the echo appears to be reflected from directly below the spacecraft,

not corrected for dispersion or possible oblique propagation effects, and is given by

h = z - c($\Delta t/2$), where z is the altitude of the spacecraft, c is the speed of light and Δt is

the time delay of the echo. Dispersion is the frequency dependent effect the plasma has

on the propagation speed of the wave relative to the speed of light. Although dispersion

corrections are important for computing the accurate electron density profiles, for our

purpose, which mainly involves identifying the location of density structures, these

corrections can be ignored. Because Mars has a distinctly non-spherical shape the

altitude, z, is computed relative to the best-fit reference ellipsoid for the surface using the parameter given by Seidelmann et al. [2002].

A spectrogram showing the apparent altitude of the ionospheric echoes for a typical ionospheric sounding pass is shown in Figure 9 where the frequency is selected to be 1.9 MHz. Spectrograms allow us to have an easier understanding of the ionosphere and especially of the oblique echoes. The oblique echoes appear as downward facing hyperbolas in a spectrogram of apparent altitude versus time. A good example of such a hyperbola-shaped echo is shown in Figure 9. The apex of the hyperbola-shaped echo in this case is at 04:57:02 UT.

3.3 Data Selection

We investigated more than 400 spectrograms and found 202 hyperbola shapes on them. Among these, 163 distinct and obvious ones were chosen for analysis. The others were considered to be too unclear to be included in the quantitative study.

CHAPTER IV
INVESTIGATION OF HYPERBOLA SHAPES ON THE
SPECTROGRAMS

We studied the echo strengths from the spectrograms. The nearly horizontal line across the spectrograms (as seen in Figure 9 at an altitude around 130 km) is due to the vertical (specular) reflections from the ionosphere of Mars. Such vertical reflections are a common feature in all of the ionospheric sounding passes on the dayside of Mars. The altitude at which the echo occurs varies with frequency and is controlled by the electron density profile in the ionosphere. In addition to commonly occurring vertical echoes from the horizontally stratified ionosphere, oblique echoes are frequently observed in the MARSIS ionospheric sounding data [Gurnett et al., 2005]. In a spectrogram of apparent altitude versus time the oblique echoes appear as downward facing hyperbola-shaped echoes. Oblique echoes consisting of half of a hyperbola are also quite common, facing either to the right or to the left with about equal probability. Among the 163 hyperbolas that have been studied in detail, 68 are full hyperbolas and the rest are half hyperbolas. So far a pattern has not been observed for different types of hyperbolas. The hyperbola shapes on the spectrograms are believed to be due to the bulges (in the case of full hyperbolas) or step-shaped changes (half hyperbolas) in the constant density surface of the ionosphere.

The ionosphere can be thought of as a horizontal mirror from which specular reflection occurs when there is an incident electromagnetic wave. The radar sends pulses in all directions. However, only the pulses which are incident perpendicularly to the constant density surfaces are reflected back to the radar. If the ionosphere density surfaces were horizontal everywhere there would be a single reflected signal from the

point right below the spacecraft. The fact that there is a second ionospheric echo implies that there is another surface perpendicular to the emitted signal. This can be explained by the existence of bulges in the ionosphere that cause the oblique echoes on the ionograms. (Figure 10 is a cartoon representation of the formation of the oblique echoes on the ionograms). The fact that the hyperbola-shaped echo must be due to oblique propagation is evident from the fact that the apparent altitude of the echo is below the main (horizontal) reflecting layer of the ionosphere, which is impossible for a purely vertical reflection, since the wave would have to pass through the region where $f_p > f$.

4.1 Evidence that the Density Structures are Fixed with Respect to Mars

That the hyperbola-shaped echoes arise from density structures which are fixed with respect to the surface of Mars has been verified by computing the apparent altitude that would occur if the radar signal reflected from a fixed point target in the ionosphere. Figure 11 shows the result of such a computation using the same data as in Figure 9. The white hyperbola-shaped line was computed by first finding the range between the spacecraft and a fixed point target using

$$R(t) = [(x(t) - x_0)^2 + (y(t) - y_0)^2 + (z(t) - z_0)^2]^{1/2}, \qquad (1)$$

and then computing the apparent altitude using $h = z(t) - R(t)$, where $x(t)$, $y(t)$ and $z(t)$ are the coordinates of the spacecraft at time t in a coordinate system fixed with respect to Mars, and x_o, y_o and z_o are the coordinates of the target. The best fit was obtained if the location the target was selected to be in the orbital plane of the spacecraft at the apex of the hyperbola (Latitude = - 4.1°, Longitude = 296.7°) and the altitude was chosen to be

the apparent altitude of the apex (Altitude = 140 km). As can be seen, the fit of the white line to the observed hyperbola-shaped echo is very good. Modeling of other comparable events also gives similar results, thereby providing strong evidence that the hyperbola-shaped echoes originated from structures in the ionosphere that are fixed with respect to Mars. In these fits, the fact that the bulges are not point reflectors is not taken into account. However, the small size of the bulges relative to the distance to the spacecraft, which is typically in the range from about 150 to 1000 km, explains why a simple point target gives a reasonably good fit to the shape of the echo.

4.2 The Vertical Positions of the Apexes of the Hyperbolas

In most cases, the apparent altitudes of the apexes of the hyperbolas extend above the ionosphere, in accordance with the assumption that they are bulges on the ionosphere. A plot of the number of events as a function of the difference, Δh, between the apparent altitude of the apex and the apparent altitude of the surrounding ionosphere at 1.8 MHz is shown in Figure 12. The root-mean-square (rms) value of Δh is 19.17 km at the given frequency and, except for one case, the maximum value is 50 km. In some cases the apexes almost merge with the ionosphere [Gurnett et al., 2005]. These measurements show the bulges are generally small compared to the distance to the spacecraft, but are large compared to the expected vertical thickness of the ionosphere. It is worth noting that there are very few cases where the apex of the hyperbola is below the ionosphere. Only 9 cases out of 163 exist where the hyperbola is below the ionosphere. Among these, only two are considerably below ($\Delta h = $ -76 km and -100 km), and seven are immediately below the ionosphere ($\Delta h = $ -2 to -6 km below). We believe that these sub-ionospheric bulges are not directly below the spacecraft, but are at an angle with respect

to the vertical and therefore are further away. There is not only a vertical distance, but also a transverse distance between the spacecraft and the position of the bulges. Since a random horizontal spatial distribution of small isotropic reflectors would give a distribution with many negative Δh values, the near absence of negative Δh values means that the density structures that give rise to the oblique echoes cannot be small hemispherical bumps. The simplest density structure that would appear to account for the observed distribution of Δh values in Figure 12 would be horizontal cylindrically shaped structures. For such a cylindrical reflector the normal incidence at closest approach would always be directly below the spacecraft, which would explain why Δh is almost never negative. It is worth mentioning that since the spacecraft is usually moving south to north when these data were collected, the cylindrical structures must have a significant east-west orientation. The apparent east-west orientation of the ionospheric density structures are seen in the magnetic maps of Mars. In Figure 13 which is a map from Connerney et al., [2005], it is possible to see this structure orientation.

CHAPTER V
THE RELATIONSHIP BETWEEN OBLIQUE ECHOES AND THE
MAGNETIC FIELD OF MARS

We believe that most of the oblique echoes from the ionosphere are the result of the electron density perturbations related to the crustal magnetic field of Mars. Mars does not have a core magnetic field, but has very complex crustal magnetic fields which were found by Mars Global Surveyor [Acuna et al., 1998; Connery et al., 1999; Ness et al., 1999]. Gurnett et al. [2005] showed that oblique echoes occur in regions of strong crustal magnetic fields, particularly when the magnetic field is vertical, either upward or downward. Most of the hyperbolas on the spectrograms appear when the vertical component of the magnetic field (B_r) is much larger than the eastward (B_φ) and southward (B_θ) components. The bottom panel of Figure 14 shows the radial, southward and eastward components of the crustal magnetic field and the field magnitude |B| computed from the Cain et al. [2003] model at an altitude of 150 km. A full hyperbola (at 01:07:20 Universal Time (UT)) with an apex point where the magnetic field has a much greater radial component can be seen in Figure 13. Also, a half hyperbola with an apex position at time t = 01:02:21UT is observed. Although the oblique echoes in Figure 13 originated from single isolated magnetic field structures, in most cases they originate from regions that have much more complex magnetic structures and correspondingly more complicated echo pattern.

One explanation for this relationship involves two geometries of magnetic field lines seen at Mars: open field lines which connect with the solar wind and closed field lines that originate on the surface and return to the surface. The basic geometry involved is illustrated in Figure 15. It is well known that a charged particle moving in a static,

uniform magnetic field moves gyrotropically along the field line. While the electrons inside closed magnetic field regions are trapped, the electrons around the vertical magnetic field areas are free to move along the magnetic field line (Krymskii et al., 2003). The solar wind electrons move easily down the open magnetic field regions and heat the ionosphere. The result is an increase in the scale height H of the ionosphere. The scale height is defined as the vertical distance upwards, over which the pressure of the atmosphere decreases by a factor of e. The scale height is given by $H = kT/mg$, where k is the Boltzmann constant, T is temperature in Kelvins, m is mean molecular mass and g is the gravitational acceleration).

To illustrate the relationship between the oblique echoes and the crustal magnetic field, Figure 16 shows the positions of the apexes of the 163 hyperbolas that were selected for study and the locations on Mars where the magnetic field is nearly vertical in the upper levels of the ionosphere. The black dots are the points where the angle between the magnetic field and vertical is smaller than 20 degrees. The magnetic fields were computed at an altitude of 150 km, using the Cain et al. [2003] model. In order to limit the comparison to regions where the magnetic field was relatively strong, only magnetic field strengths greater than 150 nT were considered. The red dots show the positions of the apexes of the hyperbolas. As can be seen the hyperbolas are almost all in the southern hemisphere, where the crustal magnetic fields are the strongest. Also, as one can see, most of the red dots are on or very close to black dots, which indicates that oblique echoes originate in regions where the crustal magnetic field is almost vertical. To confirm this relationship, the number of oblique echoes per unit solid angle, $dN / (2\pi\sin\theta d\theta)$, is plotted in Figure 17 as a function of the angle θ between the magnetic field and vertical

(or 180° - θ if the angle is greater than 90°). The plot has a large concentration of events at small angles, less than about around 12 degrees and most of the events have angle values smaller than 30°, confirming that the echoes originate from regions where the magnetic field is nearly vertical.

Finally, we questioned the possibility of a relationship between the occurrence of the oblique echoes and the downward or upward direction of the magnetic field. Of the 163 events studied, 69 of the events occur at locations where the magnetic field vector is directed downward into Mars, and 94 of them are where the magnetic field is upward out of Mars. Since the standard deviation for this number of samples is 13, the two numbers differ by only a little more than the standard deviation from the expected median value for a random distribution. Thus, there is no evidence to suggest that the occurrence of oblique echoes is related to the downward or upward directions of the magnetic field.

CHAPTER VI
CONCLUSION

In this study, we inspected more than 400 spectrograms and found 163 distinct oblique echoes in the shape of hyperbolas. The apexes of the hyperbolas identify the approximate center of the regions of enhanced electron density. The hyperbolas are inverted on the spectrograms and are either whole hyperbolas or half hyperbolas. It is suggested that these shapes can be explained by the existence of bumps in the ionosphere. Using very basic mathematical concepts, we proved that the reflections from a target fixed with respect to Mars could cause hyperbola-like shapes on the spectrograms. So, it was inferred that the reflections from the surface of a bulge on the ionosphere of Mars would cause the appearance of the hyperbolas. Statistical analyses of the apparent altitudes of the apexes of the hyperbolas, as well as analyses of repeated passes over the same region showed that there are only a few cases where the apexes of the hyperbolas are below the surrounding ionosphere, indicating that the electron density enhancements consist of horizontal cylindrical structures rather than isolated hemispherical structures. In some cases the axes of the linear density structures are found to be aligned along the axes of cylindrical magnetic field structures in the crustal magnetic field.

Also, we noticed a relationship between the hyperbola events and the crustal magnetic field of Mars. We concluded that most of the hyperbola events are observed at the places where the vertical component of the magnetic field is much stronger than other components. However, we did not find any correlation between the up or down direction of the magnetic field and the occurrence of the oblique echoes.

APPENDIX

FIGURES
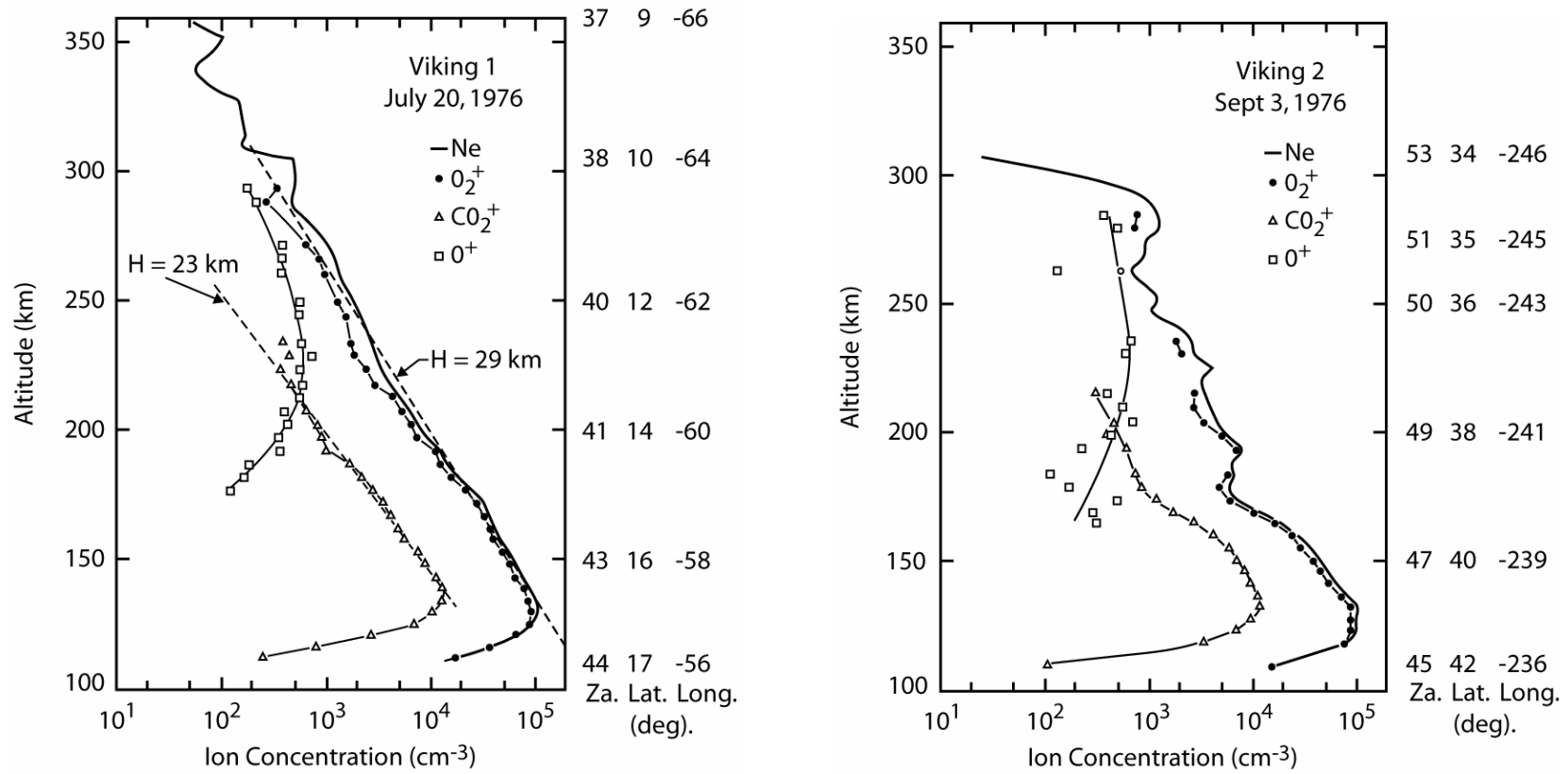
Figure A1. The altitude versus observed ion concentration plots from Viking 1 and Viking 2 data. The solid line is the total ion concentration. At the right of each graph the solar zenith angle and sublander Mars coordinates are shown.
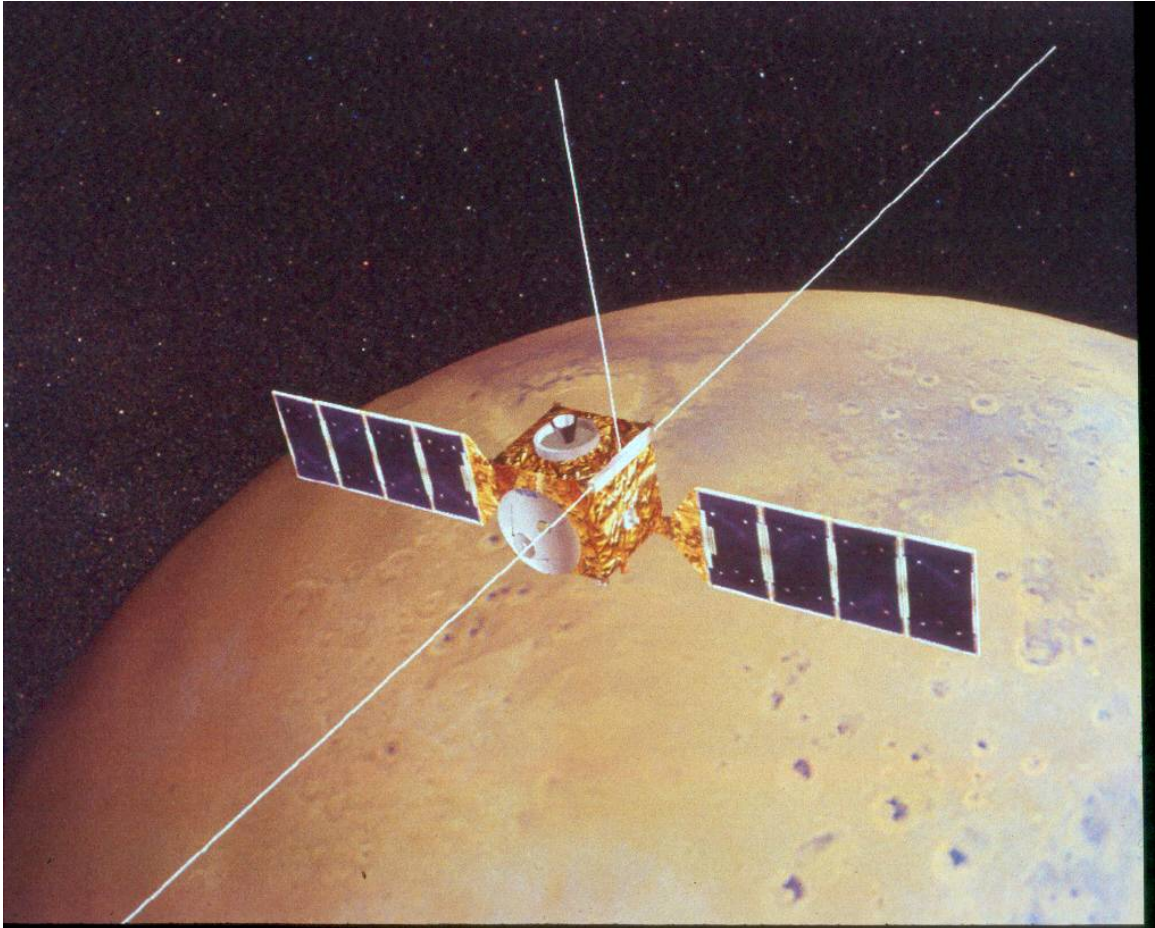
Figure A2. An artistic sketch of the Mars Express Spacecraft on its elliptic orbit around Mars.
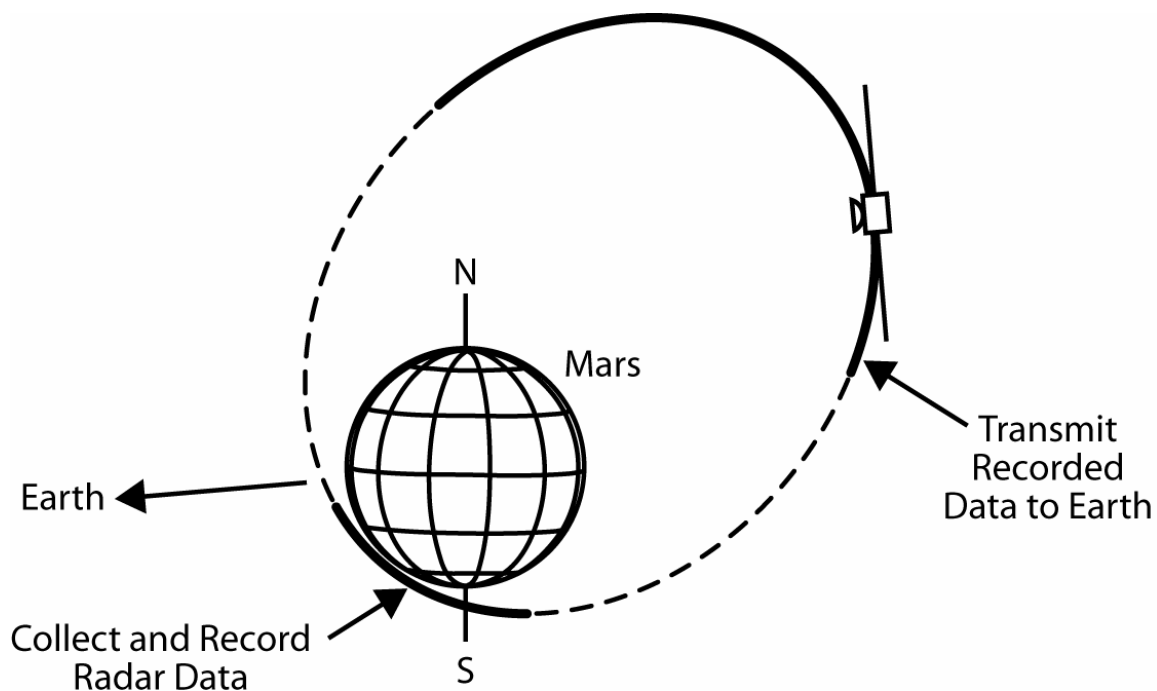
Figure A3. Collection and transmission of the data by the radar. The radar collects data at periapsis and transmits data to Earth at the apoapsis.
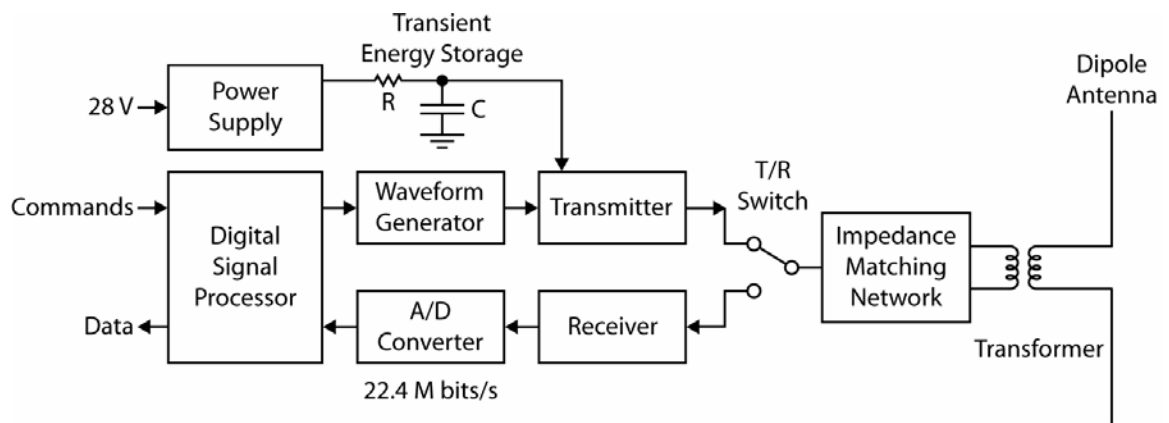
Figure A4. The electronic block diagram of MARSIS.
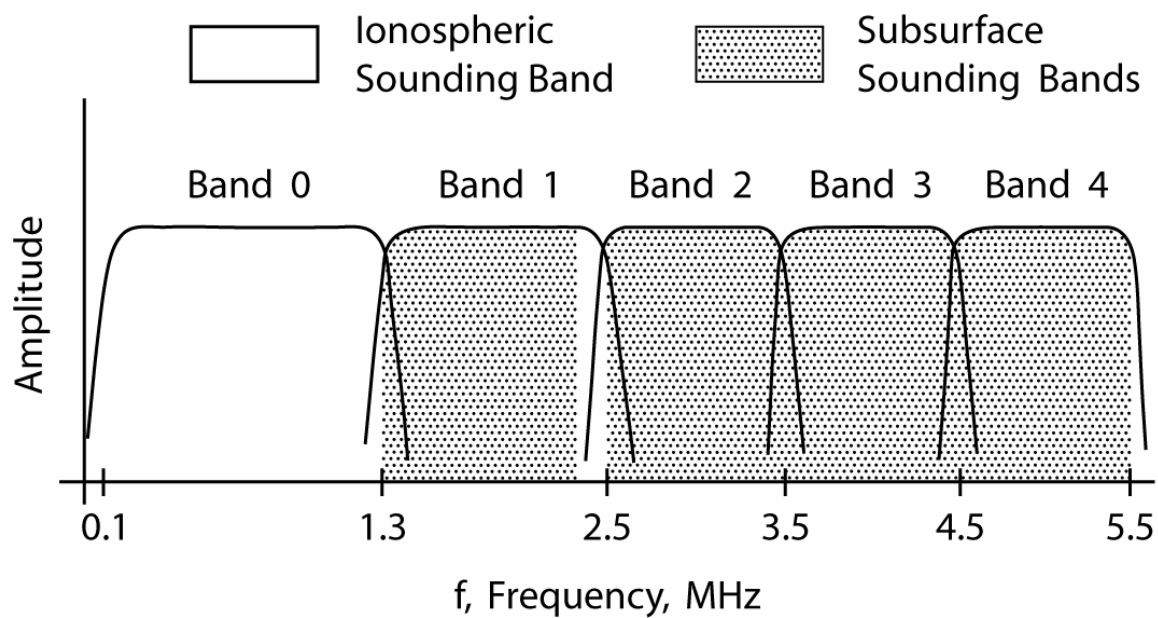
Figure A5. The five receiver bands. The first one is only for ionospheric sounding. The other four are for both ionospheric and subsurface soundings.
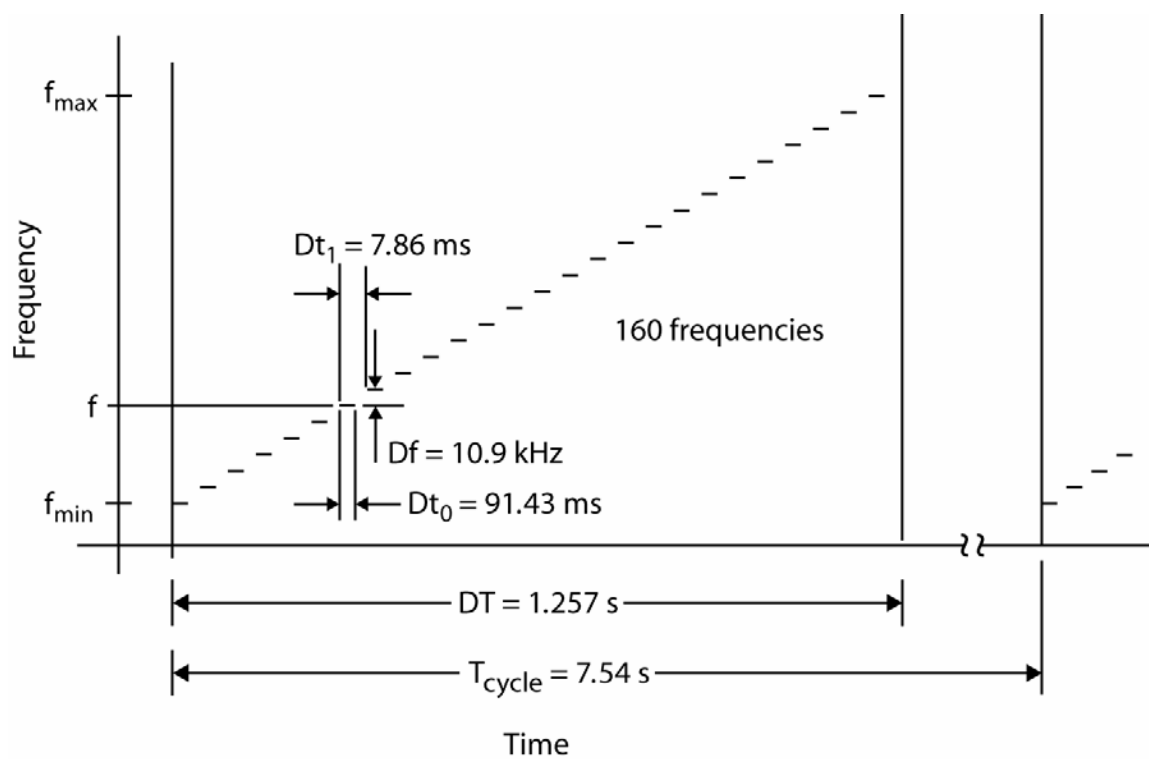
Figure A6. The frequency scan of the radar.
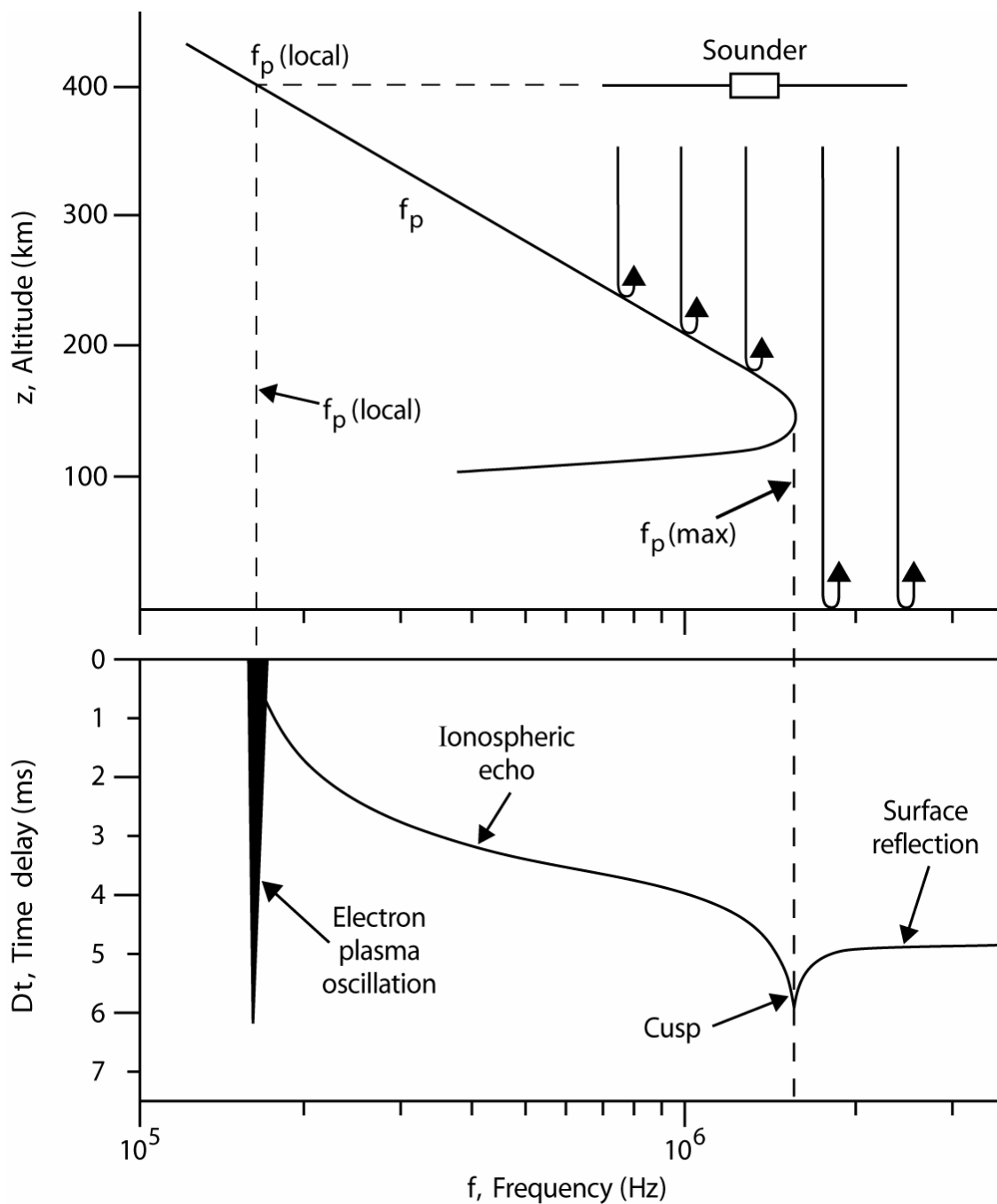
Figure A7. The top figure is a typical vertical profile of the ionospheric data which shows the apparent altitude values as a function of the frequency. The bottom one is a typical example of time delay versus frequency plot where the ionospheric echo and surface reflections are seen.
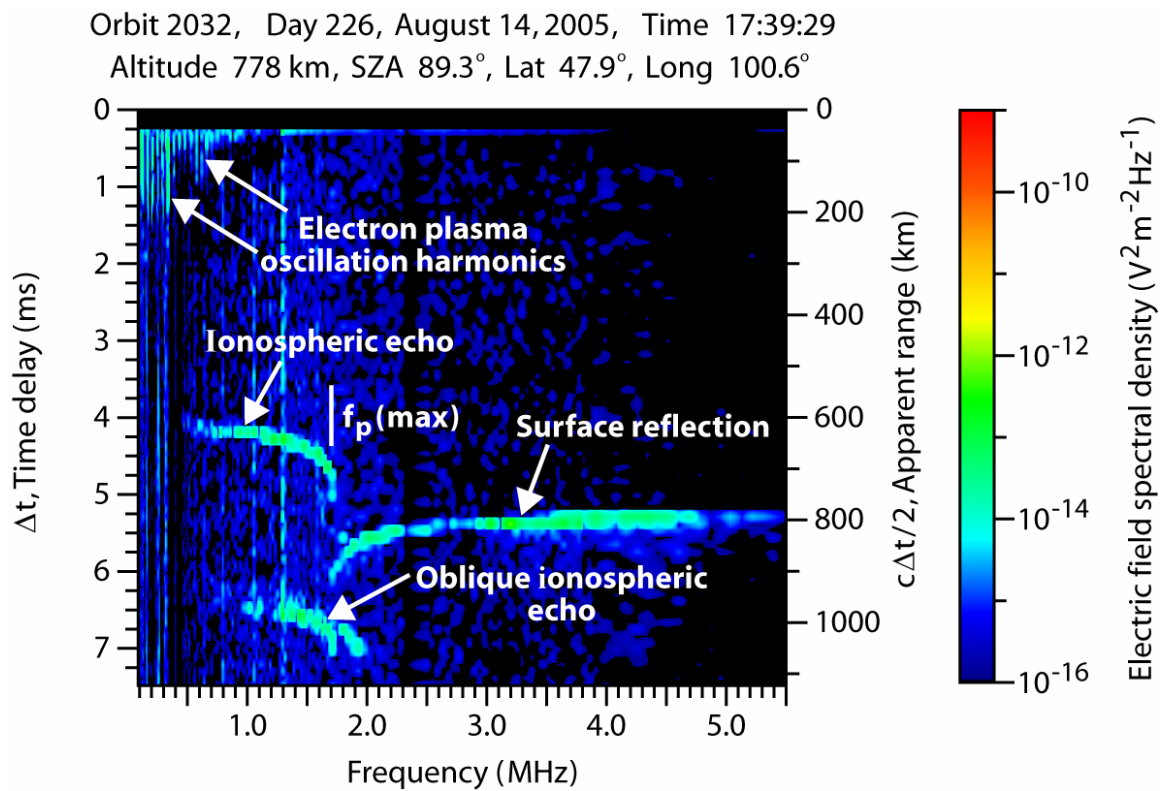
Figure A8. An example of an ionogram. The vertical and oblique ionospheric echoes as well as the surface reflection can be seen clearly.
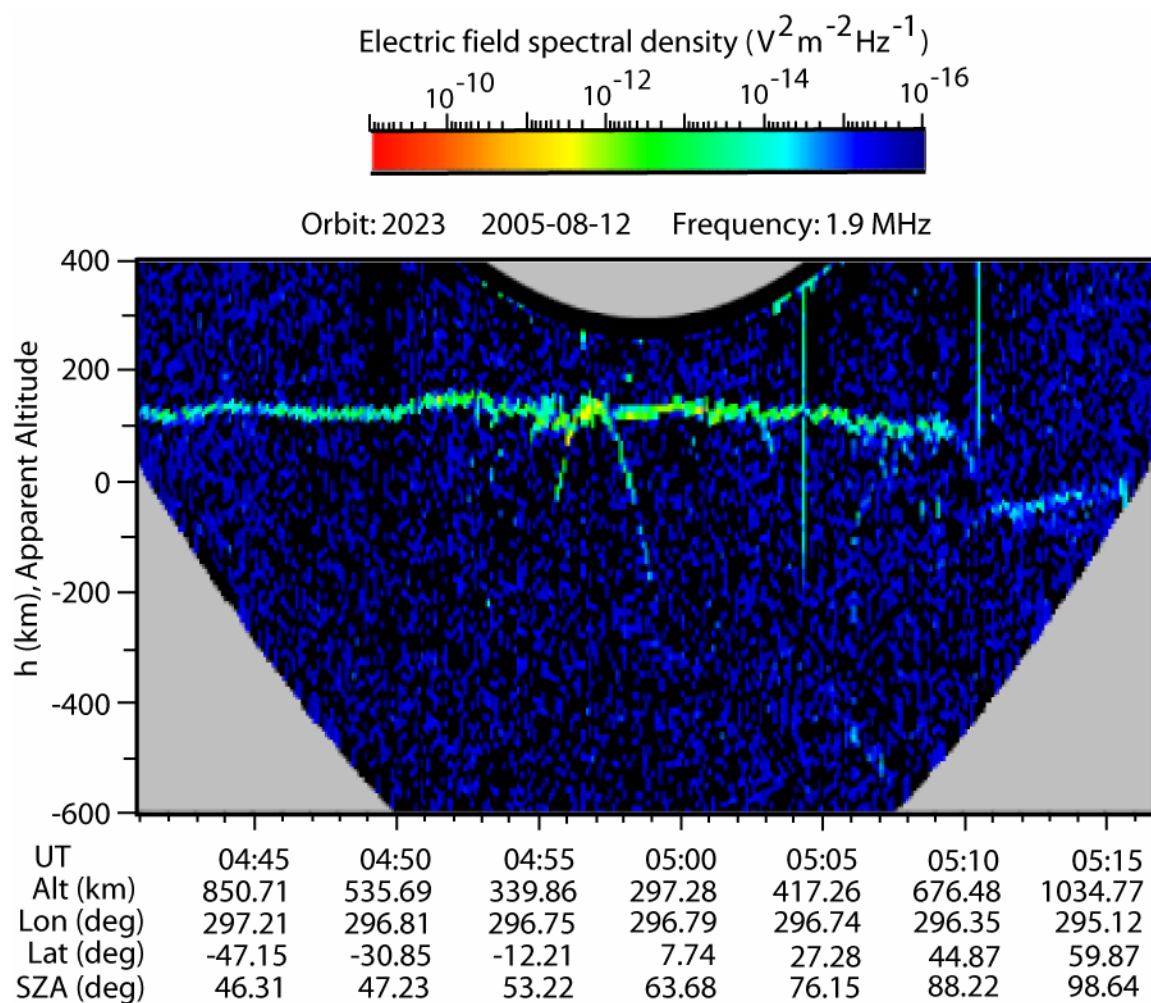
Figure A9. An example of a color–coded spectrogram of apparent altitude versus Universal Time at a frequency value of 1.9 MHz. A typical ionospheric sounding pass lasts about 36 minutes. The intensity code is shown at the top of the spectrogram. The hyperbola-shaped echo is at 04:57:02 UT.
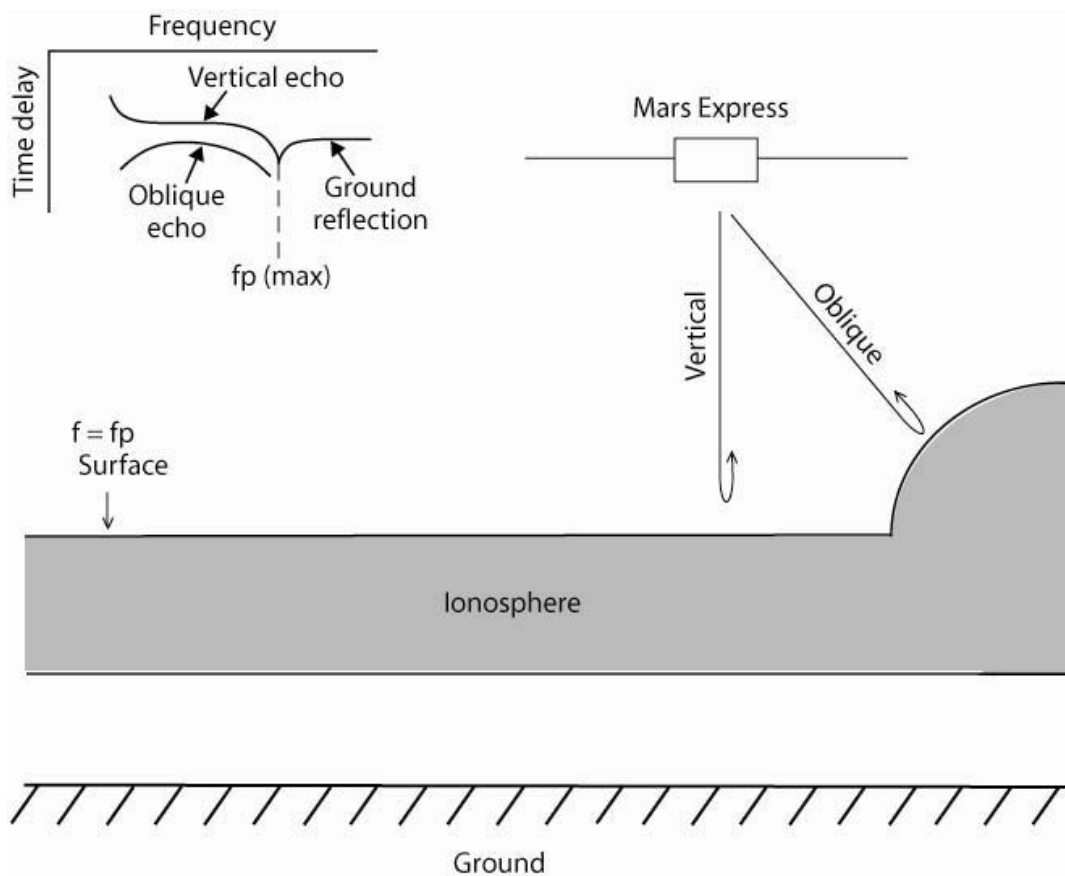
Figure A10. A sketch of the ionospheric density structure that is thought to be responsible for the oblique ionospheric echoes detected by MARSIS. As the spacecraft approaches the bulge two echoes are detected, a vertical echo from the horizontally stratified ionosphere and an oblique echo from the bulge. It is easily demonstrated that a hyperbola-shaped echo is generated by the temporal variation of the range to the reflection point as the spacecraft passes over the bulge.
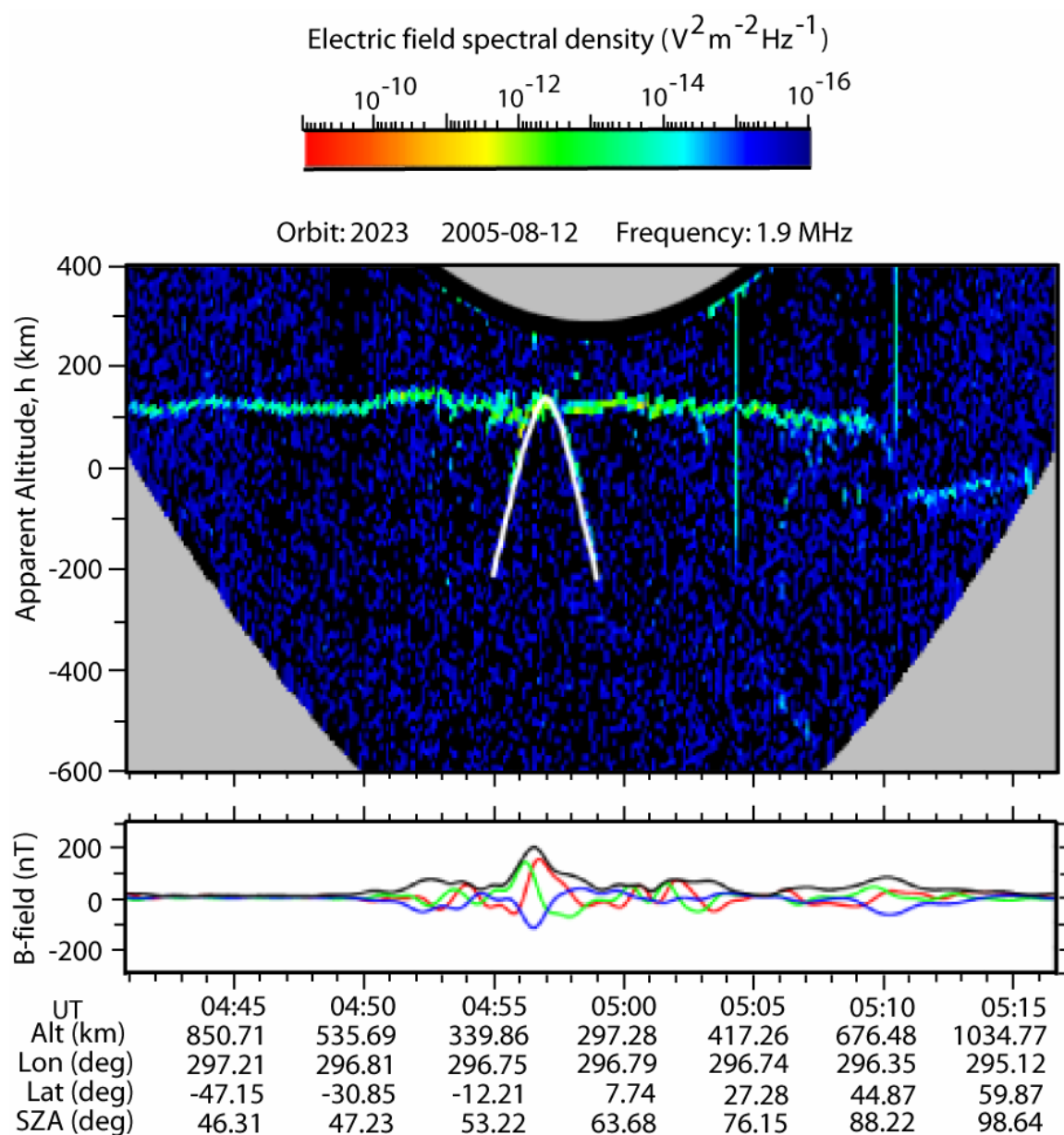
Figure A11. The apparent altitude versus time spectrogram. The white line is obtained by computing the apparent altitude that would occur if the signal is reflected from a fixed point target with respect to Mars. The observed hyperbola is in agreement with it. Lower panel shows the radial (red line), eastward (blue line) and southward (green line) components and the magnitude (black line) of the magnetic field.
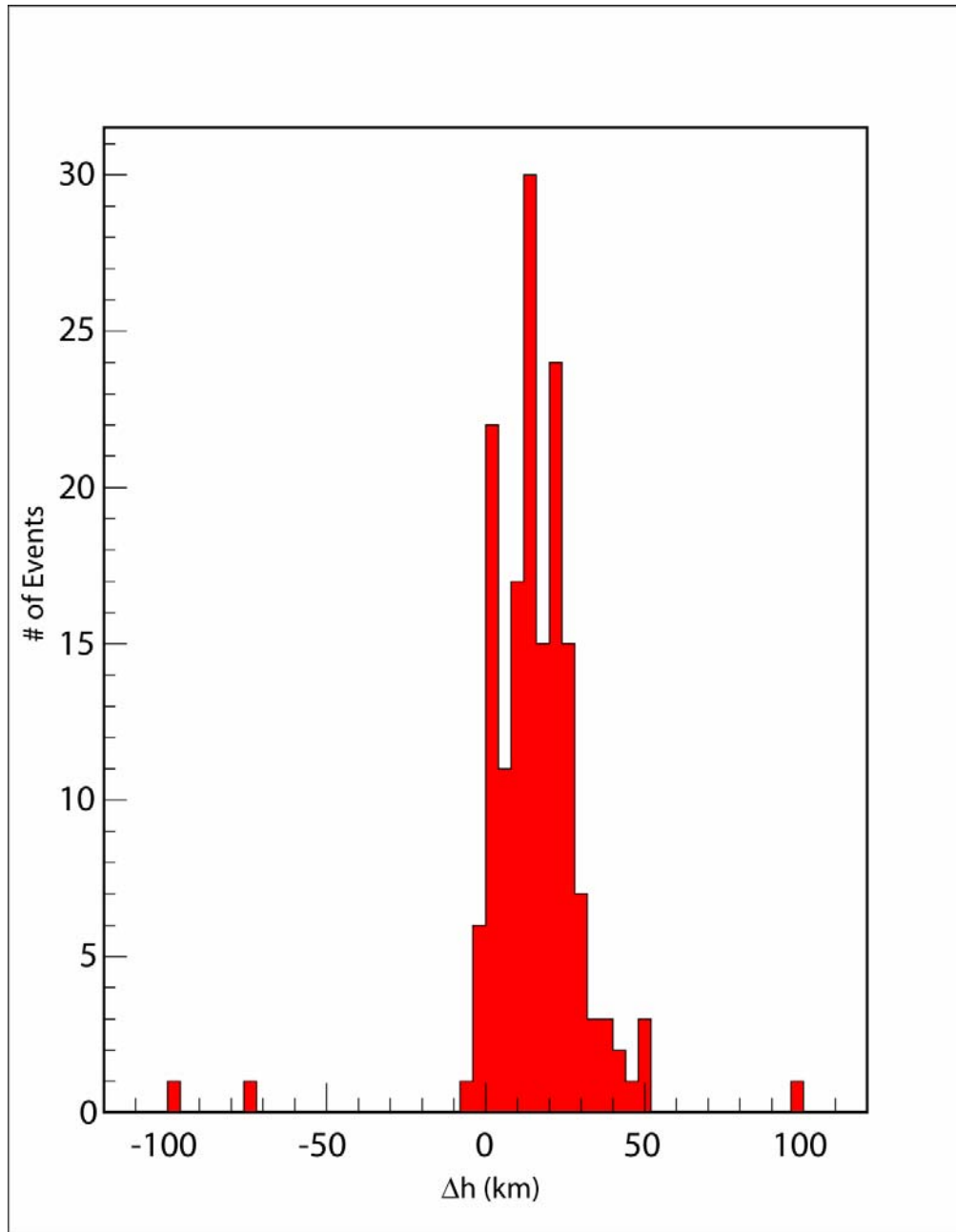
Figure A12. The histogram of the apparent altitude difference between the positions of the hyperbola apexes and the surrounding ionosphere. The mean value is 14.72 km. The near absence of negative Δh values indicates that in almost every case the spacecraft passed almost directly over the closest approach point to the bulge.

MARS CRUSTAL MAGNETISM ΔB_r **MARS GLOBAL SURVEYOR** **MAG/ER**

90°
60°
30°
0°
-30°
-60°
-90°

0° 90° 180° 270° 360°

East Longitude

UTOPIA PLANITIA
ARCADIA
ALBA PATERA
ACIDALIA
CHRYSE
ELYSIUM MONS
AMAZONIS
OLYMPUS MONS
ISIDIS
CERBERUS RUPES
THARSIS MONTES
VALLES MARINERIS
HELLAS
ARGYRE

$\Delta B_r/\Delta Lat$ (nT/deg)

-30 -10 -3 -1 -.3   +.3 1 3 10 30
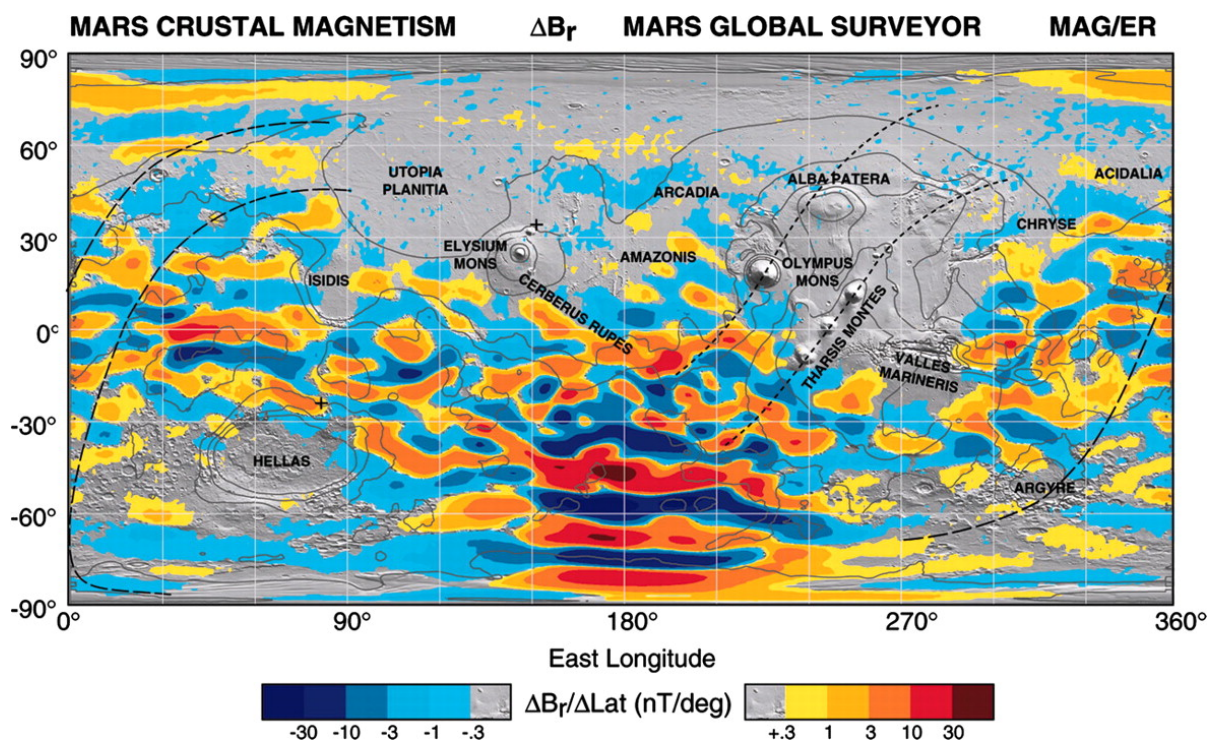
Figure A13: Map of magnetic fields of Mars observed by Mars Global Surveyor Satellite at an altitude of 400 km. In many parts of Mars, it is possible to observe the east-west structure orientation.
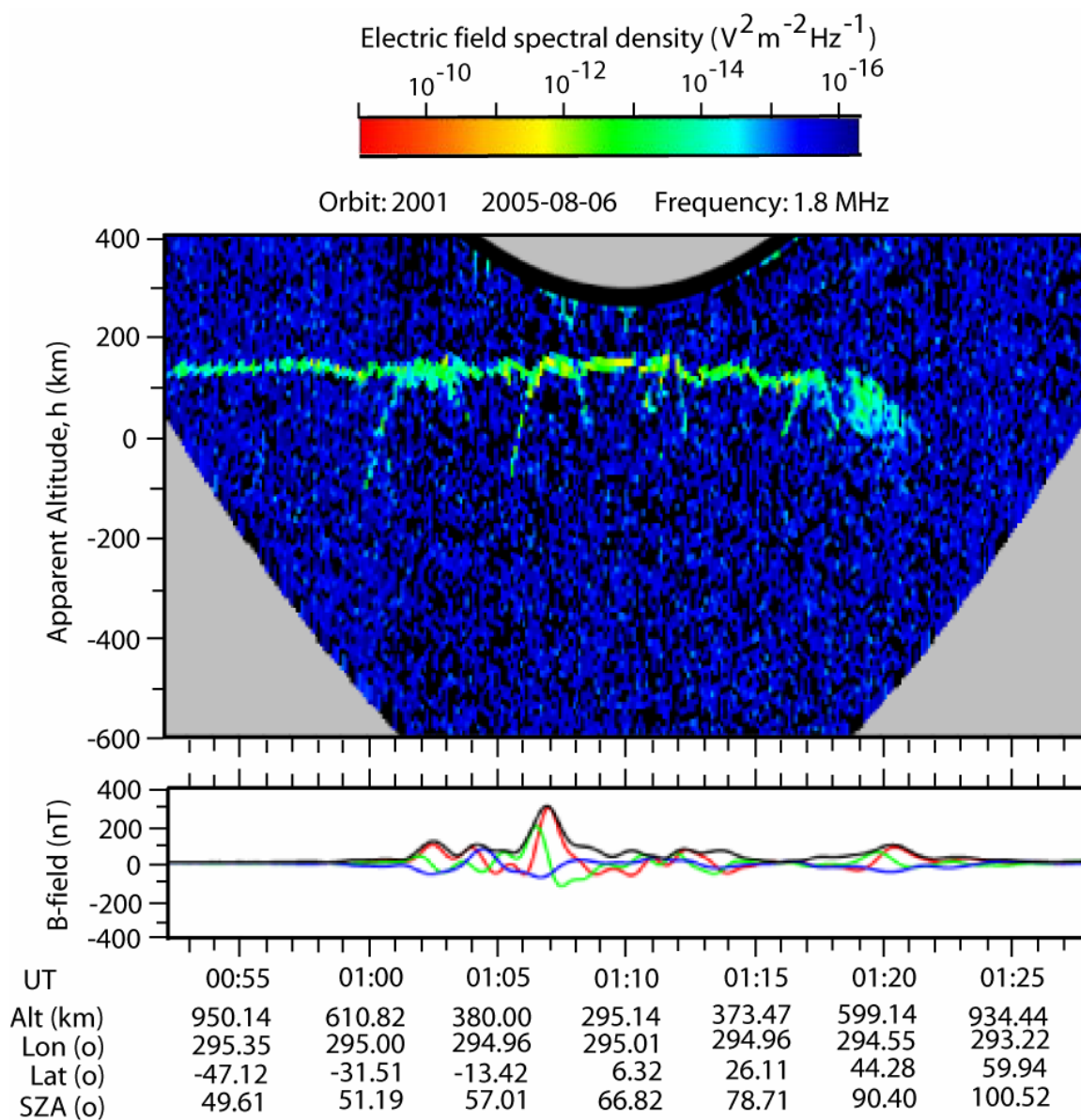
Figure A14. One half (01:02:21UT), one full (01:07:20 UT) hyperbola at the places where the magnetic field is nearly vertical are seen in this spectrogram. Lower panel shows the radial (red line), eastward (blue line) and southward (green line) components and the magnitude (black line) of the magnetic field.
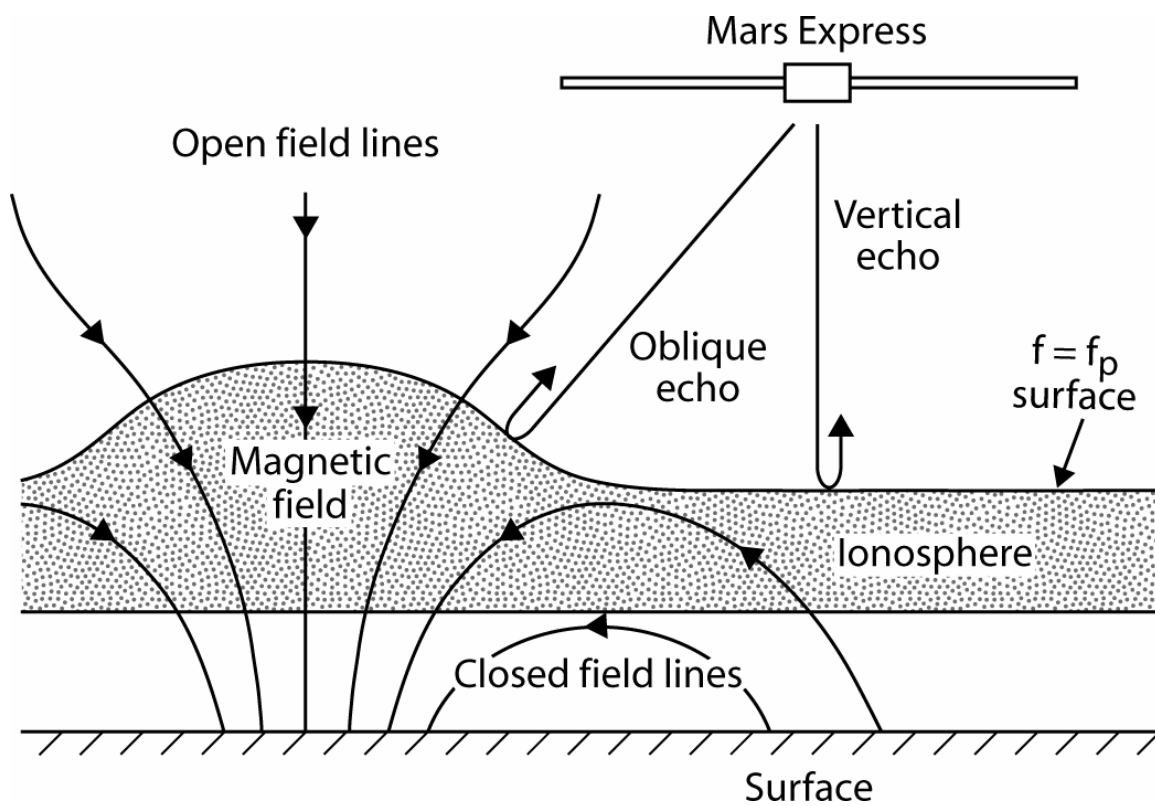
Figure A15. The cartoon showing the formation of the bulges on the ionosphere due to vertical magnetic field. The bulges are believed to cause the oblique echoes.
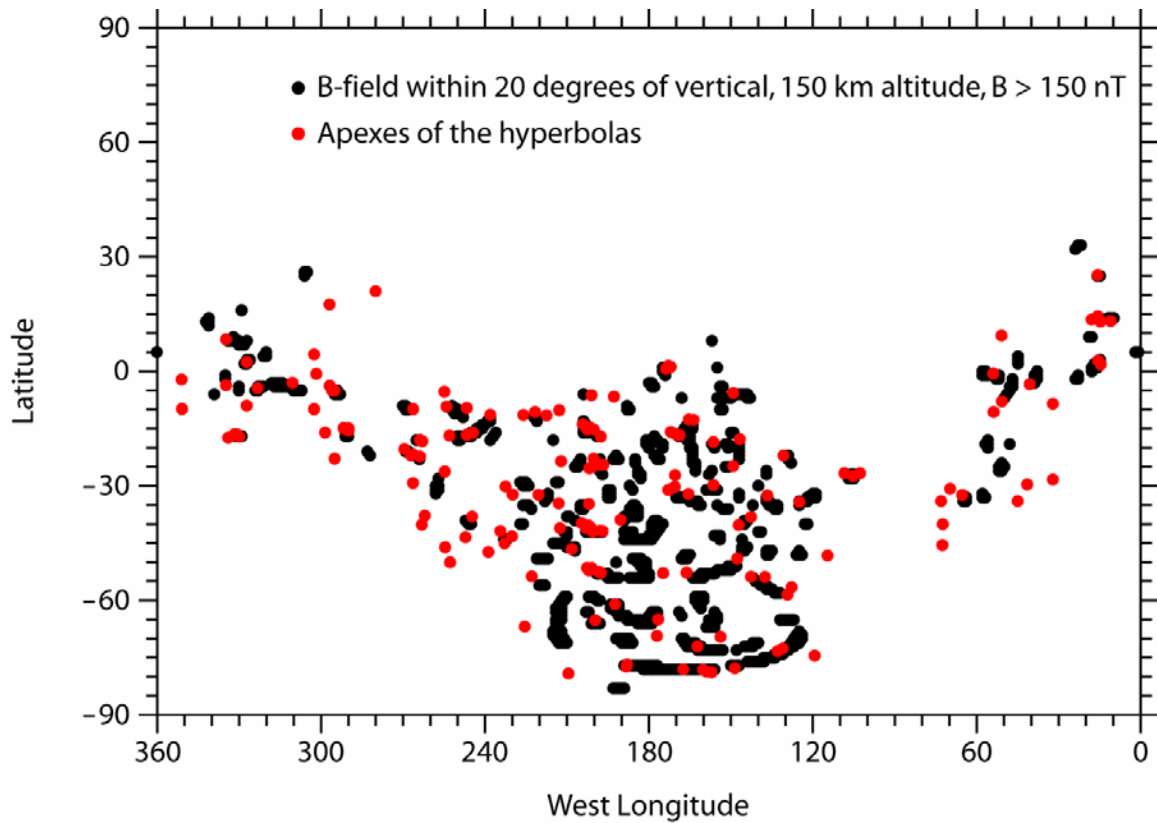
Figure A16. A latitude-longitude map of Mars showing the relationship between the origin of the oblique echoes and the magnetic field of Mars. Red dots show the positions of 163 hyperbolas and black dots are the places on the Mars where the magnetic field is within 20 degrees of vertical. Altitude is 150 km and only magnetic fields greater than 150 nT are shown. The Cain et al. (Cain et al., 2003) model is used for the magnetic field.
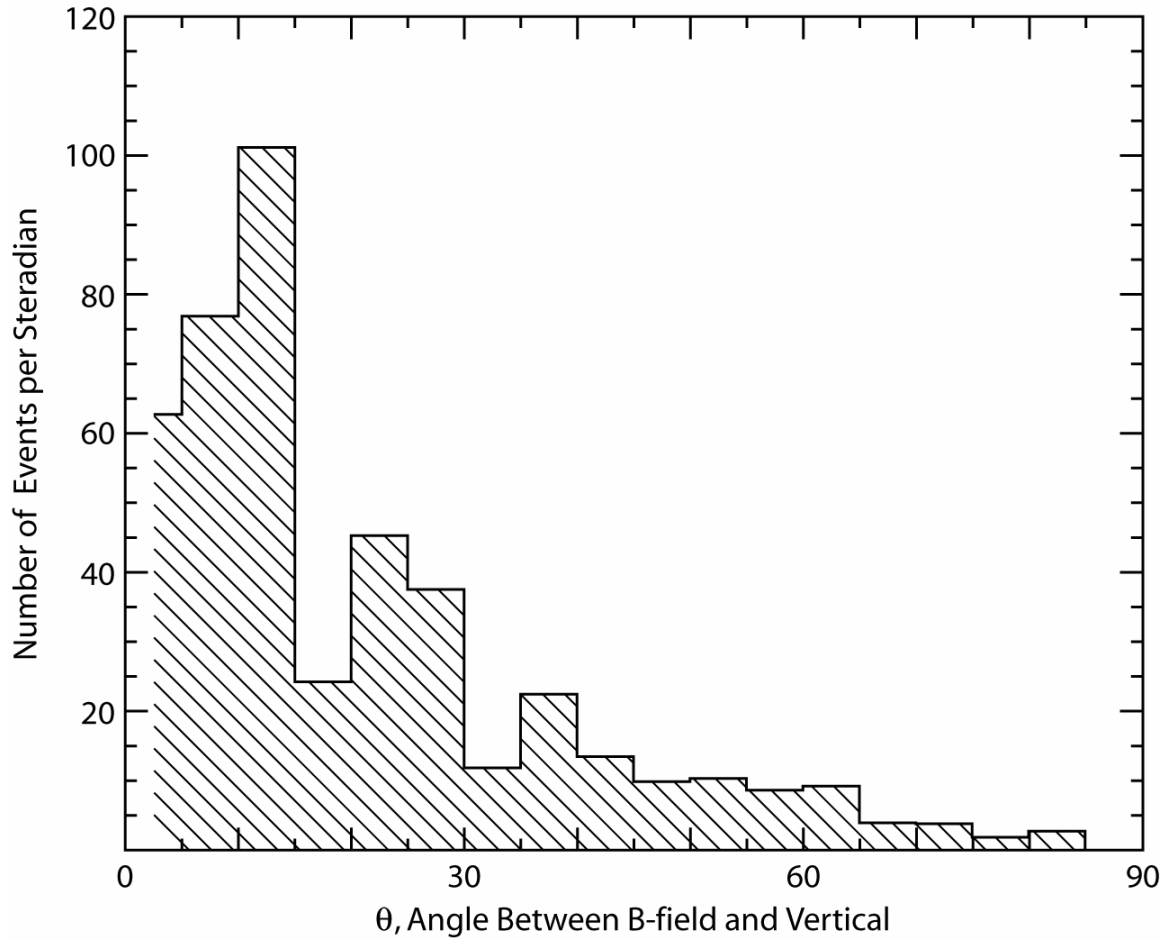
Figure A17. The number of hyperbola-shaped oblique echoes as a function of the angle between the magnetic field and the vertical at the apexes of the hyperbolas. A large peak is observed at around 12 degrees. This plot shows that oblique echoes tend to originate from regions where the magnetic field is strong and vertical.

REFERENCES

Acuna, M. H., Connerney, J. E. P., Wasilewski, P., Lin, R. P., Anderson, K. A., Carlson, C. W., McFadden, J., Curtis, D. W., Mitchell, D., Reme, H., Mazelle, C., Sauvaud, J. A., d'Uston, C., Cros, A., Medale, J. L., Bauer, S. J., Cloutier, P., Mayhew, M., Winterhalter, D., and Ness N. F., Magnetic Field and Plasma Observations at Mars: Initial Results of the Mars Global Surveyor Mission, Science, 279, 1676- 1680, 1998.

Acuna, M.H., Connerney, J. E. P., Ness, N. F., Lin, R. P., Mitchell, D., Carlson, C.W., McFadden, J., Anderson, K.A., Reme, H., Mazelle, C., Vignes, D., Wasilewski, P., Cloutier, P., Global Distribution of Crustal Magnetization Discovered by the Mars Global Surveyor MAG/ER experiment, Science, 284, 790-793, 1999.

Cain, J. C., Ferguson, B. B., Mozzoni, D., An n = 90 Internal Potential Function of the Martian Crustal Magnetic Field, J. Geophys. Res., 108 (E2), 5008, 2003.

Chicarro, A., Martin, P., Traunter, R., Mars Express: A European Mission to the Red Planet, SP-1240, pp. 3-16, European Space Agency Publication Division, Noordwijk, Nederlands, 2004.

Connerney, J.E. P., Acuna, M. H., Wasilewski, P. J., Ness, N. F., Reme, H., Mazelle, C., Vignes, D., Lin, R. P., Mitchell, D. L., and Cloutier, P. A., Magnetic Lineations in the Ancient Crust of Mars, Science, 284, 794-798, 1999.

Connerney, J.E. P., Acuna, M. H., Ness, N. F., Kletetschka, G., Mithchell, D. L., Lin, R. P., and Reme, H., Tectonic Implications of Mars Crustal Magnetism, PNAS, 102, 14970-14975, 2005.

Gurnett, D. A.and Bhattacharjee, A., Introduction to Plasma Physics with Space and Laboratory Applications, Cambridge University Press, Cambridge, 91, 2005.

Gurnett, D. A., Kirchner, D. L., Huff, R. L., Morgan, D. D., Persoon, A. M., Averkamp, T. F., Duru, F, Nielsen, E., Safaeinili, A., Plaut, J. J., and Picardi, G., Radar Soundings of the Ionosphere of Mars , Science, 310, 1929-1933, 2005.

Hanson, W. B., Sanatani, S., Zuccaro, D. R.,The Martian Ionosphere as Observed by the Viking Retarding Potential Analyzers, J. Geophys. Res., 82, 4351-4363, 1977.

Hanson, W. B. and Mantas, G. P., Viking Electron Temperature Measurements : Evidence for a Magnetic Field in the Martian Ionosphere, J. Geophys. Res., 93(A7), 7538-7544, 1988.

Krymskii, A. M., Breus, T. K, Ness, N. F., Hinson, D. P., and Bojkov, D. I., Effect of Crustal Magnetic Fieds on the Near Terminator Ionosphere at Mars: Comparison of in Situ Magnetic Field Measurements with the Data of Radio Science

Experiments on Board Mars Global Surveyor, J. Geophys. Res., 108(A12), 1431, 2003.

Luhman, J. G., and Brace, L. H., Near-Mars Space, Rev. Geophys., 29, 121, 1991.

Ness, N. F., Acuna, M. H., Connerney, J., Wasilewski, P., Mazelle, C., Sauvaud, J., Vignes, D., d'Uston, C., Reme, H., Lin, R., Mitchell, D. L., McFadden, J., Curtis, D., Cloutier, P., and Bauer, S. J., MGS Magnetic Fields and Electron Reflectometer Investigation: Discovery of Paleomagnetic Fields due to Crustal Remnance, Adv. Space Res., 23(11), 1879-1886, 1999.

Picardi, G., Biccari, D., Seu, R., Plaut, J., Johnson, W. T. K., Jordan, R. L., Safaeinili, A., Gurnett, D. A., Huff, R., Orosei, R., Bombaci, O., Calabrese, D., and Zampolini, E., Mars Express: A European Mission to The Red Planet, SP- 1240, European Space Agency Publication Division, Noordwijk, Netherlands, pp.51- 70, 2004.

Picardi, G., Plaut, J. J., Biccari, D., Bombaci, O., Calabrese, D., Cartacci, M., Cicchetti, A., Clifford, S. M., Edenhofer, P., Farrell, W. M., Federico, C., Frigeri, A., Gurnett, D. A., Hagfors, T., Heggy, E., Herique, A., Huff, R. L., Ivanov, A. B., Johnson, W. T. K., Jordan, R. L., Kirchner, D. L., Kofman, W., Leuschen, C. J., Nielsen, E., Orosei, R., Pettinelli, E., Phillips, R. J., Plettemeier, D., Safaeinili, A., Seu, R., Stofan, E . R., Vannaroni, G., D., Watters, T. R., and Zampolini, E., Radar Soundings of the Subsurface of Mars, Science, 310, 2005.

Seidelmann, P.K., Abalakin, V. K., Bursa M., Davies, M. E., De Bergh, C., Lieske, J. H., Oberst, J., Simon, J. L., Standish, E. M., Stooke, P., Thomas, P. C., Report of the IAU/IAG Working Group on Cartographic Coordinates and Rotational Elements of the Planets and Satellites: 2000, Celestial Mechanics and Dynamical Astronomy, Vol. 82, pp. 83-110, 2002.

Shinagawa, H. and Bougher, S. W., A two-dimensional MHD Model of the Solar Wind Interaction with Mars, Earth Planets Space, 51, 55-60, 1999.

Smith, E. J., Davis, L. Jr., Coleman, P. J. Jr., and Jones, D. E., Magnetic Field Measurements near Mars, Science, 149, 1241-1242, 1965.

Van Allen J. A., Frank, L. A., Krimigis, S. M., Hillis H.K., Absence of Martian Radiation Belts and Implications Thereof, Science, 149, 1228-1233, 1965.

Zhang, M. H. G., Luhmann, J. G. and Kliore, A. J., A Post Pioneer Venus Reassessment of the Martian Dayside Ionosphere as Observed by Radar Occultation Methods, J. Geophys. Res., 95, 14829-14839, 1990a.

Zhang, M. G. H., Luhmann, J. G. and Kliore, A. J., An Observational Study of the Nightside Ionosphere of Mars and Venus with Radio Occultation Methods, J. Geophys. Res., 95, 17095-17102, 1990b.